

Co-GRPO: Co-Optimized Group Relative Policy Optimization for Masked Diffusion Model

Renping Zhou^{*,1,2}, Zanlin Ni^{*,1}, Tianyi Chen¹, Zeyu Liu¹, Yang Yue¹,
Yulin Wang¹, Yuxuan Wang¹, Jingshu Liu¹, Gao Huang^{✉,1}

¹Leap Lab, Tsinghua University ²Anyverse Dynamics

Recently, Masked Diffusion Models (MDMs) have shown promising potential across vision, language, and cross-modal generation. However, a notable discrepancy exists between their training and inference procedures. In particular, MDM inference is a multi-step, iterative process governed not only by the model itself but also by various schedules that dictate the token-decoding trajectory (e.g., how many tokens to decode at each step). In contrast, MDMs are typically trained using a simplified, single-step BERT-style objective that masks a subset of tokens and predicts all of them simultaneously. This step-level simplification fundamentally disconnects the training paradigm from the trajectory-level nature of inference, leaving the inference schedules never optimized during training. In this paper, we introduce Co-GRPO, which reformulates MDM generation as a unified Markov Decision Process (MDP) that jointly incorporates both the model and the inference schedule. By applying Group Relative Policy Optimization at the trajectory level, Co-GRPO cooperatively optimizes model parameters and schedule parameters under a shared reward, without requiring costly backpropagation through the multi-step generation process. This holistic optimization aligns training with inference more thoroughly and substantially improves generation quality. Empirical results across four benchmarks—ImageReward, HPS, GenEval, and DPG-Bench—demonstrate the effectiveness of our approach. For more details, please refer to our project page: <https://co-grpo.github.io>.



Figure 1: **Qualitative and quantitative comparison of Co-GRPO against baseline approaches.** Through cooperative optimization of the MDM model and inference schedule, Co-GRPO produces images with markedly superior quality compared to baseline. Detailed prompts are provided in Table 6.

* Equal contribution. ✉ Corresponding author.

1. Introduction

Masked Diffusion Models (MDMs) have recently demonstrated remarkable success across diverse domains, including vision, language, and cross-modal applications, owing to their general-purpose modeling capabilities and significant potential for efficiency (Nie et al., 2025; Zhu et al., 2025; Ye et al., 2025; Yang et al., 2025; Liang et al., 2025).

In the visual domain, MDMs offer an efficient alternative to autoregressive (AR) models. They preserve the benefits of unified token-based multi-modal modeling (Bai et al., 2024; Xie et al., 2024a; You et al., 2025) while delivering markedly higher generation efficiency: AR models often require hundreds of sequential steps, whereas many MDMs achieve decent-quality image synthesis in only 8–16 iterations (Chang et al., 2022; 2023; Ni et al., 2024a;c). This efficiency is achieved by their parallel decoding mechanism, where generation begins from a fully masked canvas and swiftly infills multiple tokens per step. To enable this capability, MDMs adopt a BERT-style training objective (Devlin et al., 2019) that predicts all masked tokens conditioned on the visible context.

However, a fundamental discrepancy exists between the training objective and the practical inference process. Iterative generation requires a set of *inference schedules* governing the number of tokens decoded each step as well as other procedural parameters (see Table 1). These scheduling decisions, despite critically affecting final generation quality (see Table 2), are never explicitly optimized during training. Specifically, the conventional BERT-style objective simplifies training to a single-step prediction problem: masking some tokens and decode all of them at once. This *step-level* simplification circumvents the need for expensive backpropagation through the multi-step generation process but also inherently precludes the model from learning the *trajectory-level* inference schedule. As a result, the model and the inference schedule, which jointly determine the final generation quality and should ideally be optimized together, end up being separated. Practitioners must then rely on post-hoc, manually designed scheduling rules for inference, as shown in Table 1.

To address this issue, we introduce **Co-GRPO** (Co-Optimized Group Relative Policy Optimization). We formulate a new Markov Decision Process (MDP) that unifies the model and the inference schedule within a single GRPO-style policy. Leveraging the trajectory-level nature of GRPO, Co-GRPO is able to jointly optimize both components without the prohibitive cost of backpropagating through multi-step generation. This holistic view stands in sharp contrast to Naive GRPO (Luo et al., 2025; Yang et al., 2025), which inherits the conventional separation between model and schedule and optimizes only the model parameters during training. As conceptually illustrated in Figure 2, Co-GRPO instead treats model and schedule as cooperating policies driven by the same reward signal. By aligning both components to a shared objective, Co-GRPO optimizes the entire generation trajectory instead of focusing solely on model parameters, leading to significantly better performance.

Our approach achieves substantial improvements in visual quality and reward alignment for MDMs by cooperatively optimizing both the model and inference schedule, producing outputs that exhibit both superior aesthetics and enhanced prompt adherence. We demonstrate significant performance gains across four diverse text-to-image benchmarks. On reward model-based benchmarks, Co-GRPO substantially surpasses the Naive GRPO baseline method, improving ImageReward score from 0.942 to **1.122** and HPSv2 score from 28.83 to **29.37**. Moreover, the cooperatively optimized policy demonstrates strong generalization capability, achieving significant zero-shot

Inference Schedule	Predefined Function
re-mask ratio $r(t)$	$r(t) = \cos\left(\frac{t+1}{T} \cdot \frac{\pi}{2}\right)$
sample temperature $\tau_s(t)$	$\tau_s(t) = 1.0$
re-mask temperature $\tau_r(t)$	$\tau_r(t) = 2\frac{T-t}{T}$
classifier-free guidance scale $s(t)$	$s(t) = 9.0$

Table 1: An example of the manually designed inference schedule from Meissonic (Bai et al., 2024).

Table 1: An example of the manually designed inference schedule from Meissonic (Bai et al., 2024).

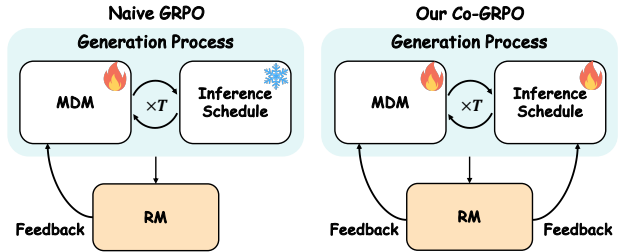


Figure 2: **Comparison between the conventional MDM post-training framework and our Co-GRPO.** Naive GRPO collects trajectories using a trainable MDM model under a fixed, predefined inference schedule. Our proposed Co-GRPO challenges this convention by cooperatively optimizing both the MDM model and the inference schedule based on the reward feedback.

improvements on both GenEval and DPG-Bench benchmarks without requiring additional fine-tuning.

Our contributions are summarized as follows:

- We identify and formalize the fundamental mismatch between the step-level BERT-style training objective and the trajectory-level inference process in MDMs, revealing that the inference schedule—despite critically affecting generation quality—remains decoupled from training and thus unoptimized in existing approaches.
- We propose Co-GRPO, a unified framework that formulates the MDM model and its inference schedule as cooperating policies within a single MDP. By leveraging trajectory-level policy gradients, Co-GRPO enables cooperative optimization of both components without the computational burden of backpropagating through multi-step generation.
- Through extensive experiments, we demonstrate that Co-GRPO substantially outperforms Naive GRPO method on reward model-based benchmarks including ImageReward and HPSv2, while exhibiting strong zero-shot generalization across diverse text-to-image benchmarks including GenEval and DPG-Bench.

2. Related Work

2.1. Image Generation Models

Diffusion models function by progressively refining an image from random Gaussian noise through a multi-step denoising process, with Stable Diffusion (Ho et al., 2020) as an early contribution and subsequent improvements in controllability and resolution (Rombach et al., 2022; Podell et al., 2023; Luo et al., 2023; Liu et al., 2024). Flow matching models (Lipman et al., 2022; Liu et al., 2022), inspired by diffusion models, generate data by learning a continuous vector field that directly transforms a simple noise distribution into the target data distribution. Transformer architectures (Saharia et al., 2022; Peebles & Xie, 2023a; Chen et al., 2024; Esser et al., 2024; Cai et al., 2025) have recently been integrated into these frameworks and have shown strong potential for performance and scalability.

Autoregressive (AR) models treat image generation as a next-token prediction task. VQ-VAE (Razavi et al., 2019) enabled the compression of images into a sequence of discrete tokens and laid the basis for a series of transformer-based AR approaches (Esser et al., 2021; Chen et al., 2018; Lee et al., 2022; Parmar et al., 2018; Team, 2024). Recent studies proposed the unification of language and visual modalities, extending text comprehension and reasoning abilities to text-to-image synthesis (Wu et al., 2025; Deng et al., 2025; Fang et al., 2025). However, AR models suffer from a major computational bottleneck during high-resolution generation (Cui et al., 2025; Wang et al., 2025a) and a discount in performance due to the unidirectional prior introduced by causal attention.

Masked diffusion models (MDMs) frame image synthesis as a mask prediction problem where all the masked visual tokens are decoded in a small, fixed number of steps, enabling remarkably fast inference. MaskGIT (Chang et al., 2022) pioneered this masked image modeling approach and demonstrated high fidelity and diversity. Subsequent works (Ni et al., 2024a;b;c; 2025) have investigated various approaches to improve MaskGIT’s generation efficiency. This concept was later extended to text-to-image (T2I) generation (Li et al., 2023; Chang et al., 2023; Bai et al., 2024) and to the unification of understanding and generation (Li et al., 2024; Xie et al., 2024b). Given their recent advances, MDMs represent a highly promising direction for research and deserve further exploration.

2.2. RL in Text-to-Image Generation

Reinforcement learning (RL) has proven effective across diverse domains, from mathematical reasoning and code generation (Lee et al., 2023; Shao et al., 2024) to visual perception (Wang et al., 2025b; Chen et al., 2025b), demonstrating its versatility in optimizing non-differentiable decision processes. In image generation, RL is a powerful paradigm for aligning outputs with human preferences. Policy gradient methods such as PPO (Schulman et al., 2017) serve as a foundational class of algorithms in this domain. DPOK (Fan et al., 2023) and DDPO (Black et al., 2023) adapted them to diffusion models, enabling fine-tuning based on downstream reward functions without requiring differentiable metrics. DPO and its variants (Rafailov et al., 2023; Wallace et al., 2024; Yuan et al., 2024; Liang et al., 2024; Zhang et al., 2025) reformulated the objective to learn directly from preference data. Most recently, GRPO-based methods (Shao et al., 2024) have emerged as a promising direction. Previous work (Sun et al., 2025) demonstrated GRPO’s effectiveness on diffusion models, while Flow-GRPO (Liu et al.,

2025) and DanceGRPO (Xue et al., 2025) adapted the framework to flow matching models. MMaDA (Yang et al., 2025) and Mask-GRPO (Luo et al., 2025) further extended it to MDMs, proposing preliminary techniques to estimate the transition probabilities. Our work builds upon this approach and seeks to further enhance the model’s performance.

3. Preliminaries

3.1. Masked Diffusion Models for T2I Generation

Let $\mathbf{V} \in \{1, \dots, V\}^N$ denote a sequence of discrete image tokens and c the conditional prompt. A Masked Diffusion Model (MDM) aims to learn the data distribution $p_{\text{data}}(\mathbf{V}|c)$ by progressively refining an initially fully-masked sequence, denoted as $([\mathbb{M}], \dots, [\mathbb{M}])$, through a series of denoising steps. At each denoising step t , the model predicts a conditional distribution over the next state:

$$\mathbf{V}^{(t)} \sim p_{\theta,t}(\cdot | \mathbf{V}^{(t-1)}, c), \quad (1)$$

where θ represents the model parameters. This distribution is estimated via a two-stage procedure:

1. **Sampling step.** For each position i , a new token $V_i^{(t)}$ is sampled or retained:

$$V_i^{(t)} = \begin{cases} \sim p_{\theta, \tau_s(t), s(t)}(V_i | \mathbf{V}^{(t-1)}, c), & \text{if } V_i^{(t-1)} = [\mathbb{M}], \\ V_i^{(t-1)}, & \text{otherwise,} \end{cases} \quad (2)$$

where the $\tau_s(t)$ and $s(t)$ are the sampling temperature and the classifier-free guidance scale, respectively.

Simultaneously, a confidence score $C_i^{(t)}$ is assigned to the newly sampled tokens:

$$C_i^{(t)} = \begin{cases} \log p(V_i = \hat{V}_i^{(t)} | \mathbf{V}^{(t-1)}, c), & \text{if } V_i^{(t-1)} = [\mathbb{M}], \\ +\infty, & \text{otherwise.} \end{cases} \quad (3)$$

2. **Remask step.** Let $\tau_r(t)$ and $r(t)$ be the given re-mask temperature and re-mask ratio. The re-masking distribution is defined as:

$$\hat{p}_{\tau_r(t)} \propto \text{Softmax}(C^{(t)} / \tau_r(t)). \quad (4)$$

We sample a set of indices $U^{(t)} \subseteq \{1, \dots, N\}$ containing $\lceil r(t) N \rceil$ tokens according to $\hat{p}_{\tau_r(t)}$. Selected positions are re-masked to $[\mathbb{M}]$ for subsequent refinement:

$$V_i^{(t)} \leftarrow [\mathbb{M}] \quad \forall i \in U^{(t)}. \quad (5)$$

For a comprehensive description of the sampling and re-mask procedures, please refer to (Ni et al., 2024a).

3.2. Group Relative Policy Optimization (GRPO) for MDMs

Reinforcement Learning (RL) is formally described by a discounted Markov Decision Process (MDP) defined by the tuple $(\mathcal{S}, \mathcal{A}, \mathcal{P}, \rho_0, R, \gamma)$, where \mathcal{S} is the state space, \mathcal{A} is the action space, $\mathcal{P}(s'|s, a)$ is the transition kernel, $\rho_0(s)$ is the initial-state distribution, $R : \mathcal{S} \times \mathcal{A} \rightarrow \mathbb{R}$ is the reward function, and $\gamma \in [0, 1)$ is the discount factor. The objective in the RL framework is to find an optimal policy π^* that maximizes the expected discounted return:

$$\pi^* \in \arg \max_{\pi} \mathbb{E}_{\tau \sim \pi} \left[\sum_{t=0}^{\infty} \gamma^t R(s_t, a_t) \right], \quad (6)$$

where the expectation is taken over the trajectory distribution $\tau = (s_0, a_0, s_1, a_1, \dots)$ induced by the policy π and the environment dynamics.

We formulate the MDM generative process into a finite-horizon MDP with horizon T . The components are formally defined as follows:

$$\begin{aligned} s_t &\triangleq (\mathbf{V}^{(t)}, c), \quad a_t \triangleq \mathbf{V}^{(t+1)}, \\ p(s_{t+1}|s_t, a_t) &\triangleq (\delta_c, \delta_{\mathbf{V}^{(t+1)}}), \\ p(a_t | s_t) &\triangleq \pi_{\text{model}, t} = p_{\theta, t}(\mathbf{V}^{(t+1)} | \mathbf{V}^{(t)}, c). \end{aligned} \quad (7)$$

The model policy $\pi_{\text{model},t}$ is the conditional token prediction policy. $\delta_x(\cdot)$ denotes the Dirac delta function centered at x , which implies that the state transition is deterministic given the action a_t . The reward $R(s_t, a_t)$ is sparse, provided only at the terminal step $T - 1$, and evaluates the quality of the completed sequence $\mathbf{V}^{(T)}$ against the condition c .

For GRPO training, accurate estimation of the likelihood of $\pi_{\text{model},t}$ is crucial. Since the action a_t only involves sampling new tokens at the currently masked positions, prior work (Huang et al., 2025; Luo et al., 2025) approximates the single-step log-likelihood based on the joint probability distribution of the tokens decoded in this step. Let $I_t^{\text{fill}} = \{i \mid V_i^{(t)} = [\text{M}] \text{ and } V_i^{(t+1)} \neq [\text{M}]\}$ be the set of indices where a token was sampled. The policy log-likelihood is approximated as the product of independent probabilities:

$$\pi_{\text{model},t} \approx \prod_{i \in I_t^{\text{fill}}} p_{\theta} \left(V_i^{(t+1)} \mid \mathbf{V}^{(t)}, c \right). \quad (8)$$

The standard GRPO objective function is given by:

$$\mathcal{L}_{\theta} = -\frac{1}{G} \frac{1}{T} \sum_{g=1}^G \sum_{t=0}^{T-1} [\min \left(r_t^g(\theta) A_t^g, \text{clip}(r_t^g(\theta), 1 - \epsilon, 1 + \epsilon) A_t^g \right) + \beta \mathbb{D}_{\text{KL}}(\pi_{\theta} \parallel \pi_{\text{ref}})], \quad (9)$$

where $r_t^g(\theta)$ is the probability ratio, defined as:

$$r_t^g(\theta) = \frac{\pi_{\theta,t}(a_t^g | s_t^g)}{\pi_{\theta_{\text{old}},t}(a_t^g | s_t^g)} \quad (10)$$

$$= \prod_{i \in I_t^{\text{fill}}} \frac{p_{\theta} \left(V_{g,i}^{(t+1)} \mid \mathbf{V}_g^{(t)}, c \right)}{p_{\theta_{\text{old}}} \left(V_{g,i}^{(t+1)} \mid \mathbf{V}_g^{(t)}, c \right)}. \quad (11)$$

Here, $\pi_{\theta_{\text{old}},t}$ is the policy used for trajectory collection. π_{ref} is the reference model used for KL regularization, and A_t^g is the group advantage estimated from the normalized reward.

4. Method

4.1. From Naive GRPO to Co-GRPO

In this section, we introduce our Co-Optimized Group Relative Policy Optimization (Co-GRPO) framework, which extends the standard Markov Decision Process (MDP) for Masked Diffusion Models (MDMs). The core idea of Co-GRPO is to treat the inference schedule—specifically, sampling temperature τ_s , classifier-free guidance scale s , re-mask temperature τ_r , and re-mask ratio r (denoted collectively as \mathcal{A})—not as fixed hyperparameters, but as trainable actions selected by the agent at each denoising step.

Formally, we formulate this unified, finite-horizon MDP with the following components:

$$s_t \triangleq (\mathbf{V}^{(t)}, c), \quad a_t \triangleq \left(\mathbf{V}^{(t+1)}, \mathcal{A}_{t+1} \right),$$

$$p(s_{t+1} | s_t, a_t) \triangleq (\delta_c, \delta_{\mathbf{V}^{(t+1)}}),$$

$$p(a_t | s_t) \triangleq p_{\theta, \phi, t}(\mathbf{V}^{(t+1)}, \mathcal{A}_{t+1} | \mathbf{V}^{(t)}, c).$$

(12)

Here, the state s_t consists of the current tokens $\mathbf{V}^{(t)}$ and conditional prompt c . The action a_t is now a composite tuple containing both the next visual tokens $\mathbf{V}^{(t+1)}$ and the next inference schedule \mathcal{A}_{t+1} . Critically, the joint policy $p(a_t | s_t)$ is parameterized by both the MDM θ and the scheduling policy ϕ . This perspective expands the original action space of the MDP to co-optimize both the visual tokens and the schedule itself.

This formulation modularly encapsulates the conventional Naive-GRPO. Specifically, if the policy component for the schedule is set to a *fixed*, pre-defined function, i.e., $\mathcal{A}_t \equiv \mathcal{A}_{\text{fixed}}(t)$, our Co-GRPO framework precisely reduces to the Naive-GRPO formulation (Equation (7)).

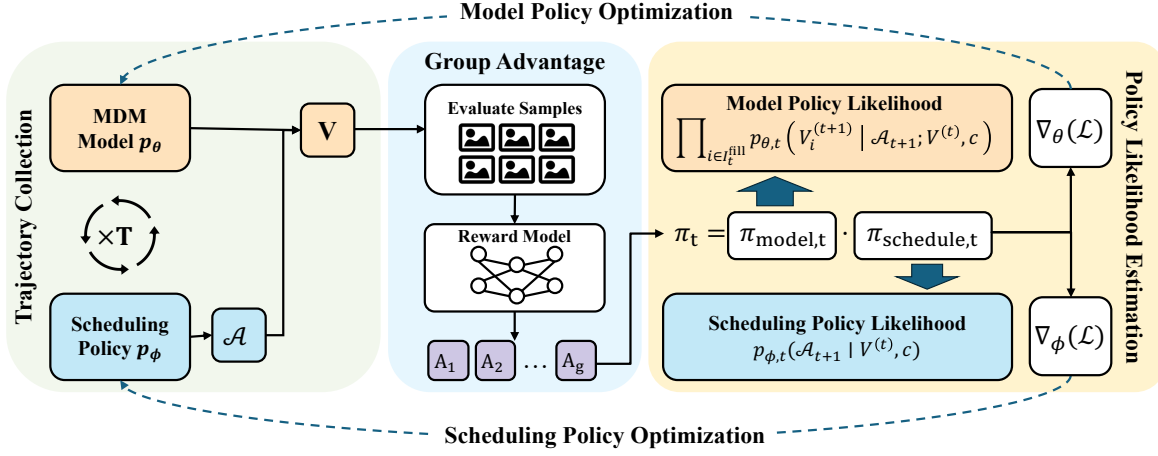


Figure 3: **Overview of our proposed Co-GRPO.** During the trajectory collection phase, both the sampled visual tokens (\mathbf{V}) and their associated inference schedule (\mathcal{A}) are collected at each step. These trajectories are evaluated by the reward model, and the resulting scores are aggregated and normalized at the group level to compute individual advantages. In the subsequent policy optimization phase, the joint policy is explicitly factorized into a *model policy* π_θ and a *scheduling policy* π_ϕ . By estimating their respective likelihoods and applying an alternating optimization strategy, our approach enables the cooperative refinement of both policies toward improved generation quality.

However, this fixed-schedule assumption is a significant limitation. To illustrate the sensitivity of the schedule, we conducted a simple experiment (Table 2). We tested a cosine schedule for the mask ratio, $r_t = \cos\left(\frac{t+1}{T}\right)^\gamma$, varying only the exponent γ . The results show that minor changes in the schedule lead to significant variations in evaluation metrics.

Motivated by this finding, we move beyond fixed schedule and formalize \mathcal{A} as a trainable action. This leads to a factorization of the joint policy $p(a_t|s_t)$ from Equation (12):

$$\begin{aligned} p(a_t|s_t) &\triangleq p_{\theta,\phi,t}(\mathbf{V}^{(t+1)}, \mathcal{A}_{t+1} | \mathbf{V}^{(t)}, c) \\ &= p_{\theta,t}(\mathbf{V}^{(t+1)} | \mathcal{A}_{t+1}; \mathbf{V}^{(t)}, c) \cdot p_{\phi,t}(\mathcal{A}_{t+1} | \mathbf{V}^{(t)}, c) \\ &= \pi_{\text{model},t} \cdot \pi_{\text{schedule},t} \end{aligned} \quad (13)$$

Here, $\pi_{\text{model},t}$ is the model policy, analogous to the policy in Naive-GRPO, which now generates $\mathbf{V}^{(t+1)}$ conditioned on the dynamically chosen schedule \mathcal{A}_{t+1} . The second term, $\pi_{\text{schedule},t}$, is the new scheduling policy that learns to select \mathcal{A}_{t+1} based on the current state s_t .

We model the scheduling policy $\pi_{\text{schedule},t}$ as a multivariate Gaussian distribution, whose mean is predicted by a network, to parameterize the continuous components of \mathcal{A} :

$$\pi_{\text{schedule},t} = p_{\phi,t}(\mathcal{A}_{t+1} | \mathbf{V}^{(t)}, c) \sim \mathcal{N}(\eta_\phi(s_t), \sigma \mathbf{I}), \quad (14)$$

where $\eta_\phi(s_t)$ is a network parameterized by ϕ that predicts the mean of the distribution, and σ is a fixed hyper-parameter controlling the policy's exploration variance.

This extended MDP exposes both the denoising network (θ) and the scheduling network (ϕ) to the same reinforcement signal. Consequently, the Co-GRPO framework optimizes a unified clipped surrogate objective:

$$\mathcal{L}_{\theta,\phi} = -\frac{1}{G} \frac{1}{T} \sum_{g=1}^G \sum_{t=0}^{T-1} [\min(r_t^g(\theta, \phi) A_t^g, \text{clip}(r_t^g(\theta, \phi), 1 - \epsilon, 1 + \epsilon) A_t^g) + \beta \mathbb{D}_{\text{KL}}(\pi_{\theta,\phi} \| \pi_{\text{ref}})], \quad (15)$$

where the probability ratio $r_t^g(\theta, \phi)$ is based on joint policy:

$$r_t^g(\theta, \phi) = \frac{\pi_{\theta, \phi, t}(a_t^g | s_t^g)}{\pi_{\theta_{\text{old}}, \phi_{\text{old}}, t}(a_t^g | s_t^g)}. \quad (16)$$

The objective explicitly allows gradients to flow to both model θ and schedule ϕ . This enables the denoising network and its own inference schedule to *co-adapt* simultaneously, optimizing for the expected return.

4.2. Alternating Co-Optimization Strategy

As depicted in Figure 3, our Co-GRPO (Co-Optimized Group Relative Policy Optimization) framework aims to jointly train the denoising model (θ) and the scheduling policy (ϕ). The foundation for this joint training lies in the factorization of the joint policy likelihood (Equation (13)), which estimates the trajectory based on both the model’s token generation and the schedule’s action selection.

A naive, simultaneous optimization, however, presents a significant challenge. Specifically, the denoising model (θ) contains vastly more parameters than the scheduling policy (ϕ). Yet, as demonstrated in our preliminary experiment (Table 2), the low-dimensional ϕ has a large impact on generation quality. This asymmetry—a small impact on ϕ and a large impact on θ —leads to a stable training dynamic when both θ and ϕ are updated simultaneously (see Table 5d).

To address this challenge, we propose to leverage the separability inherent in our policy factorization (Equation (13)). We revisit the joint probability ratio r_t^g (denoted as r_t in the subsequent derivation for notational simplicity) and decompose it according to our factorization:

$$r_t(\theta, \phi) = \frac{\pi_{\theta, \phi, t}(a_t | s_t)}{\pi_{\theta_{\text{old}}, \phi_{\text{old}}, t}(a_t | s_t)} = \frac{\pi_{\text{model}, t} \cdot \pi_{\text{schedule}, t}}{\pi_{\text{old model}, t} \cdot \pi_{\text{old schedule}, t}} = \frac{\pi_{\text{model}, t}}{\pi_{\text{old model}, t}} \cdot \frac{\pi_{\text{schedule}, t}}{\pi_{\text{old schedule}, t}} \quad (17)$$

where

$$\frac{\pi_{\text{model},t}}{\pi_{\text{old model},t}} = \frac{p_{\theta,t}(\mathbf{V}^{(t+1)} \mid \mathcal{A}_{t+1}; \mathbf{V}^{(t)}, c)}{p_{\theta_{\text{old}},t}(\mathbf{V}^{(t+1)} \mid \mathcal{A}_{t+1}; \mathbf{V}^{(t)}, c)} \quad (18)$$

$$= \prod_{i \in I_t^{\text{fill}}} \frac{p_{\theta, t} \left(V_i^{(t+1)} \mid \mathcal{A}_{t+1}; \mathbf{V}^{(t)}, c \right)}{p_{\theta_{\text{old}}, t} \left(V_i^{(t+1)} \mid \mathcal{A}_{t+1}; \mathbf{V}^{(t)}, c \right)}, \quad (19)$$

is independent of the scheduling control parameters ϕ once \mathcal{A}_{t+1} is determined, and

$$\frac{\pi_{\text{schedule},t}}{\pi_{\text{old schedule},t}} = \frac{p_{\phi,t}(\mathcal{A}_{t+1} \mid \mathbf{V}^{(t)}, c)}{p_{\phi_{\text{old}},t}(\mathcal{A}_{t+1} \mid \mathbf{V}^{(t)}, c)}, \quad (20)$$

is also independent of the model parameters θ . In other words, the two sets of trainable parameters θ and ϕ are highly separable in our optimization objective.

Driven by this observation, we propose an alternative optimization strategy that decouples the training into distinct phases. The optimization alternates between N_m iterations of model parameter updates and N_s iterations of schedule updates. In this scheme, we modify the probability ratio r_t used in the Co-GRPO objective (Equation (15)) based on the current phase. Formally, within a single update cycle ($n = 1, \dots, N_m + N_s$), the ratio is defined as:

$$r_t(\theta, \phi) = \begin{cases} \frac{\prod_{i \in I_t^{\text{fill}}} p_{\theta, t} \left(V_i^{(t+1)} | \mathcal{A}_{t+1}; \mathbf{V}^{(t)}, c \right)}{\prod_{i \in I_t^{\text{fill}}} p_{\theta_{\text{old}}, t} \left(V_i^{(t+1)} | \mathcal{A}_{t+1}; \mathbf{V}^{(t)}, c \right)} & n < N_m \\ \frac{p_{\phi, t}(\mathcal{A}_{t+1} | \mathbf{V}^{(t)}, c)}{p_{\phi_{\text{old}}, t}(\mathcal{A}_{t+1} | \mathbf{V}^{(t)}, c)} & \text{otherwise.} \end{cases} \quad (21)$$

Model	Params	ImageReward	HPS v2.0				
			Animation	Concept-art	Painting	Photo	Averaged
Diffusion-based Models							
SD v1.4 (Rombach et al., 2022)	0.9B	0.087	27.26	26.61	26.66	27.27	26.95
SD v2.0 (Rombach et al., 2022)	0.9B	0.174	27.48	26.89	26.86	27.46	27.17
Dreamlike Photoreal 2.0 (Art, 2023)	0.9B	0.168	28.24	27.60	27.59	27.99	27.86
DeepFloyd-XL (DeepFloyd, 2023)	5.5B	0.453	27.64	26.83	26.86	27.75	27.27
SDXL Base 1.0 (Podell et al., 2023)	3.5B	0.790	28.88	27.88	27.92	28.31	28.25
SDXL Refiner 1.0 (Podell et al., 2023)	6.6B	0.886	28.93	27.89	27.90	28.38	28.27
DALL-E 3 (Betker et al., 2023)	-	1.094	29.09	28.07	28.15	28.41	28.43
Majicmix Realistic v7 (Merjic, 2023)	0.9B	0.126	27.88	27.19	27.22	27.64	27.48
Pixart- α (Chen et al., 2024)	0.6B	1.115	29.30	28.57	28.55	28.99	28.85
Deliberate (Desync, 2024)	1.5B	0.285	28.13	27.46	27.45	27.62	27.67
Realistic Vision (SG_161222, 2024)	1.1B	1.088	28.22	27.53	27.56	27.75	27.77
OmniGen (Xiao et al., 2025)	3.8B	1.055	29.22	28.25	28.43	28.89	28.70
Token-based Models							
Show-o (Xie et al., 2024b)	1.3B	1.028	28.90	28.34	28.40	28.47	28.53
BLIP3o-NEXT (Chen et al., 2025a)	3.0B	0.926	28.32	27.43	27.53	28.44	27.93
MaskGen-XL (Kim et al., 2025)	1.1B	0.797	28.25	27.98	27.83	27.78	27.96
Meissonic (Bai et al., 2024)	1.0B	0.942	29.57	28.58	28.72	28.45	28.83
Meissonic + Co-GRPO	1.0B	1.122(+0.18)	29.70(+0.13)	29.62(+1.04)	29.12(+0.40)	29.03(+0.58)	29.37(+0.54)

Table 3: Quantitative results on reward model based benchmarks ImageReward (Xu et al., 2023) and HPSv2 (Wu et al., 2023).

This approach ensures that each component is optimized with respect to a stable counterpart, significantly improving convergence behavior and overall performance. The ablation study in Table 5d also proves this point.

5. Experiments

5.1. Implementation Details

5.1.1. TRAINING STRATEGY

We trained our Co-GRPO model utilizing a composite reward signal derived from two model-based reward: ImageReward (Xu et al., 2023) and HPSv2 (Wu et al., 2023). The advantage calculation employed a weighted linear combination of these two components, with both models contributing equally (a weight of 0.5 for each component) to the total advantage.

The base text-to-image model employed is Meissonic (Bai et al., 2024), a high-performance Masked Diffusion Model. Consistent with the default configuration of Meissonic, the number of inference steps was fixed at 48 throughout the reinforcement learning training process. The Kullback-Leibler (KL) divergence regularization coefficient β was set to 0, consistent with prior reinforcement learning studies applied to MDMs (Luo et al., 2025; Huang et al., 2025). Further detailed hyperparameter configurations and the specific network architectures pertaining to the alternative co-optimization strategy are provided in the Section A.

5.1.2. EVALUATION DETAILS

During evaluation, the model’s inference step count is fixed at 48 to maintain consistency with the training setup. Performance under varying step counts is further investigated and presented in Table 5b. We report the model’s performance on the ImageReward and HPSv2 rewards. The former consists of 500 prompts, and the latter contains approximately 3,000 prompts. The HPSv2 rewards are further categorized into four distinct image categories: Animation, Concept-art, Painting, and Photo. Additionally, to demonstrate the model’s generalization capability, we test its performance on two established general text-to-image benchmarks GenEval (Ghosh et al., 2023) and DPG-Bench (Hu et al., 2024).

5.2. Main Results

The results presented in Table 3 demonstrate that our method substantially improves the ImageReward and HPSv2 rewards while introducing only a marginal increase in learnable parameters. Specifically, Co-GRPO training delivers notable performance gains: ImageReward increases by 0.18 and the HPSv2 reward improves by 0.54, outperforming all reported baselines. Notably, our 1B-parameter model surpasses models with significantly larger number of parameters, underscoring the superior efficiency and effectiveness of our approach in aligning with human preferences.

Furthermore, Table 4 demonstrates the strong generalization capability of our model on established text-to-image evaluation benchmarks. Importantly, Co-GRPO is trained without using any prompts or reward signals from GenEval or DPG-Bench, making this a zero-shot evaluation setting. Despite this, our method achieves substantial improvements, elevating the GenEval score from 0.47 to 0.55 and the DPG-Bench score from 64.57 to 70.10. These gains on unseen benchmarks demonstrate that Co-GRPO learns generalizable human preference alignment that transfers effectively to diverse text-to-image generation tasks.

5.3. Ablation Study

Table 5 presents the comprehensive results of the ablation.

Component of Trainable Action Space Results in Table 5a demonstrate a monotonic improvement in both the ImageReward and HPSv2 as more components of the action space are progressively made trainable. Optimizing only the model parameters (*i.e.*, the Naive GRPO formulation in Equation (7)) yields only marginal gains in generation quality. In contrast, introducing the scheduling policy within the Co-GRPO framework leads to substantial performance improvements. Moreover, progressively incorporating additional components of the inference schedule produces steady, incremental gains, indicating that each component provides tangible gains to the overall model performance.

Optimization Strategy Table 5d compares the Alternative optimization strategy with the Joint optimization strategy, controlling for an identical total number of training iterations. While the Joint approach also improves model performance, its effect is less significant than the Alternative method. This validates the intuition discussed in Section 4.2 and underscores the superiority and necessity of the Alternative training approach for optimizing. Table 5c illustrates the impact of the number of alternating optimization cycles on training efficacy. We observe a substantial performance leap after the initial cycle, and subsequent cycles further reinforce the model’s performance. In our experiments, performance largely converges after three cycles.

Transfer Capability Analysis We analyze the transferability of our learned policy across different inference settings. In Table 5b, we evaluate a model trained for 48 steps under both fewer (8) and more (64) inference steps. The scheduling policy is transferred between different step counts using interpolation. We find that our method yields a consistent improvement over the baseline at all tested step counts, with the performance gain being especially prominent at smaller step counts. This result demonstrates the model’s generalizability concerning the number of inference steps and suggests that the learned scheduling policy may be more critical for achieving high-quality generation under low-step conditions. In Table 5e, we evaluate the model’s performance against other reward models (MPS (Zhang et al., 2024) and Clip-Score (Ilharco et al., 2021)). The model shows consistent performance gains across these metrics, which demonstrates strong generalization ability across various external reward models.

Model	Params	GenEval	DPG-Bench
DALL-E mini (Dayma et al., 2021)	0.4B	0.23	-
DALL-E 2 (Ramesh et al., 2022)	3.5B	0.52	-
SD v1.5 (Rombach et al., 2022)	0.9B	0.43	63.18
SD v2.1 (Rombach et al., 2022)	0.9B	0.50	68.09
LlamaGen (Sun et al., 2024)	0.8B	0.32	65.16
Chameleon (Team, 2024)	7.0B	0.39	-
Meisisonic (Bai et al., 2024)	1.0B	0.47	64.57
Meisisonic + Co-GRPO	1.0B	0.55(+0.08)	70.10(+6.53)

Table 4: Quantitative results on general prompt-adherence benchmarks. Our model is trained under the same configuration as the main experiment using the ImageReward and HPSv2 reward models, and evaluated in a zero-shot setting on the GenEval (Ghosh et al., 2023) and DPG-Bench (Hu et al., 2024) benchmarks without relying on external distilled data or ground-truth detectors.

Table 4 demonstrates the strong generalization capability of our model on established text-to-image evaluation benchmarks. Importantly, Co-GRPO is trained without using any prompts or reward signals from GenEval or DPG-Bench, making this a zero-shot evaluation setting. Despite this, our method achieves substantial improvements, elevating the GenEval score from 0.47 to 0.55 and the DPG-Bench score from 64.57 to 70.10. These gains on unseen benchmarks demonstrate that Co-GRPO learns generalizable human preference alignment that transfers effectively to diverse text-to-image generation tasks.

Model	Schedule				ImageReward	HPSv2	Steps		ImageReward			HPSv2		
	r	τ_r	τ_s	s			Test	Train	Baseline	Ours	Δ	Baseline	Ours	Δ
✓					0.942	28.83	8	48	0.133	0.874	0.741	26.42	28.61	2.19
✓	✓				1.014	28.86	16	48	0.735	1.053	0.318	28.03	29.23	1.20
✓	✓	✓			1.037	28.93	32	48	0.902	1.091	0.189	28.62	29.23	0.61
✓	✓	✓	✓		1.070	29.09	48	48	0.942	1.122	0.180	28.83	29.37	0.54
✓	✓	✓	✓	✓	1.102	29.21	64	48	0.941	1.099	0.158	28.80	29.39	0.59
✓	✓	✓	✓	✓	1.122	29.37								

(a) Comparison on the component of trainable action space.

(b) Comparison of transfer capability on different inference steps.

Cycle	ImageReward	HPSv2
0	0.942	28.83
1	1.067	29.21
2	1.093	29.22
3	1.122	29.37

Strategy	ImageReward	HPSv2
Baseline	0.942	28.83
Joint	1.031	29.06
Alternative	1.122	29.37

Method	MPS	Clip-Score
Baseline	13.47	31.94
Co-GRPO	14.05	32.35
Δ	0.58	0.41

(c) Comparison on alternative training cycles.

(d) Comparison on training strategies.

(e) Comparison on transfer capability to different reward models.

Table 5: **Ablation studies.** We mark our default settings in gray .

5.4. Visualization Results

Figure 4 provides qualitative comparisons between images generated by our approach, the base model, and the GRPO-optimized model. Across a wide range of prompts, Co-GRPO produces outputs with consistently finer details and higher visual fidelity. Furthermore, in specific instances, such as the prompt “A black and white cat looking out a window over another cat”, the generated image demonstrate stronger prompt adherence. This indicates that Co-GRPO improves prompt following along with better aesthetics. The enhanced visual quality and semantic accuracy collectively demonstrate the effectiveness of jointly optimizing both the model and inference schedule.

6. Conclusion

In this paper, we present Co-GRPO, a GRPO-based framework that substantially improves MDMs performance on text-to-image generation. Our work is driven by the insight that the inference schedule—an essential yet previously underexplored component of the MDM generation process—plays a pivotal role in generation performance. To address this, we reformulated the underlying MDP to incorporate the scheduling policy, establishing the basis for our unified Co-GRPO framework. Building on this formulation, we further developed the mathematical formulation for a Co-Optimization Strategy that jointly optimizes the inference schedule and model parameters. Our approach yields significant improvements and generalization results across diverse rewards and benchmarks, highlighting the importance of co-optimization during post-training.

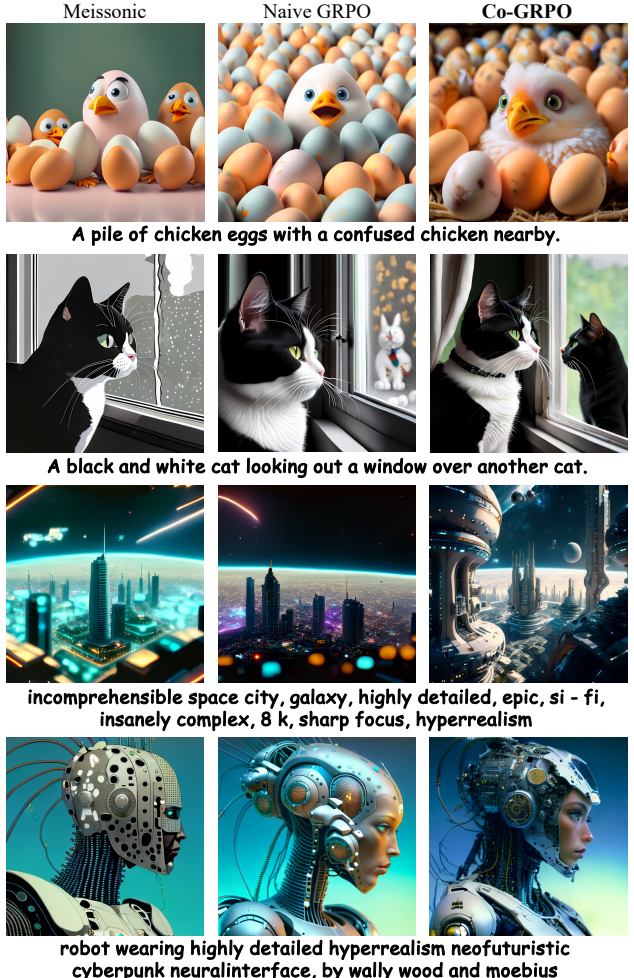


Figure 4: Qualitative comparisons of the base model and models optimized with GRPO and Co-GRPO. Co-GRPO generates images with superior aesthetics while better preserving fine-grained visual details compared to both the base model and GRPO.

References

Art, D. Dreamlike photoreal 2.0. <https://huggingface.co/dreamlike-art/dreamlike-photoreal-2.0>, 2023.

Bai, J., Ye, T., Chow, W., Song, E., Chen, Q.-G., Li, X., Dong, Z., Zhu, L., and Yan, S. Meissonic: Revitalizing masked generative transformers for efficient high-resolution text-to-image synthesis. In *The Thirteenth International Conference on Learning Representations*, 2024.

Betker, J., Goh, G., Jing, L., Brooks, T., Wang, J., Li, L., Ouyang, L., Zhuang, J., Lee, J., Guo, Y., et al. Improving image generation with better captions. *Computer Science*. <https://cdn.openai.com/papers/dall-e-3.pdf>, 2(3):8, 2023.

Black, K., Janner, M., Du, Y., Kostrikov, I., and Levine, S. Training diffusion models with reinforcement learning. *arXiv preprint arXiv:2305.13301*, 2023.

Cai, Q., Chen, J., Chen, Y., Li, Y., Long, F., Pan, Y., Qiu, Z., Zhang, Y., Gao, F., Xu, P., et al. Hidream-11: A high-efficient image generative foundation model with sparse diffusion transformer. *arXiv preprint arXiv:2505.22705*, 2025.

Chang, H., Zhang, H., Jiang, L., Liu, C., and Freeman, W. T. Maskgit: Masked generative image transformer. In *Proceedings of the IEEE/CVF conference on computer vision and pattern recognition*, pp. 11315–11325, 2022.

Chang, H., Zhang, H., Barber, J., Maschinot, A., Lezama, J., Jiang, L., Yang, M.-H., Murphy, K. P., Freeman, W. T., Rubinstein, M., et al. Muse: Text-to-image generation via masked generative transformers. In *International Conference on Machine Learning*, pp. 4055–4075. PMLR, 2023.

Chen, J., Yu, J., Ge, C., Yao, L., Xie, E., Wang, Z., Kwok, J. T., Luo, P., Lu, H., and Li, Z. Pixart- α : Fast training of diffusion transformer for photorealistic text-to-image synthesis. In *ICLR*, 2024.

Chen, J., Xue, L., Xu, Z., Pan, X., Yang, S., Qin, C., Yan, A., Zhou, H., Chen, Z., Huang, L., et al. Blip3o-next: Next frontier of native image generation. *arXiv preprint arXiv:2510.15857*, 2025a.

Chen, X., Mishra, N., Rohaninejad, M., and Abbeel, P. Pixelsnail: An improved autoregressive generative model. In *International conference on machine learning*, pp. 864–872. PMLR, 2018.

Chen, Z., Luo, X., and Li, D. Visrl: Intention-driven visual perception via reinforced reasoning. *arXiv preprint arXiv:2503.07523*, 2025b.

Cui, Y., Chen, H., Deng, H., Huang, X., Li, X., Liu, J., Liu, Y., Luo, Z., Wang, J., Wang, W., et al. Emu3. 5: Native multimodal models are world learners. *arXiv preprint arXiv:2510.26583*, 2025.

Dayma, B., Patil, S., Cuenca, P., Saifullah, K., Abraham, T., Lê Khắc, P., Melas, L., and Ghosh, R. Dall-e mini, 7 2021. URL <https://github.com/borisdayma/dalle-mini>.

DeepFloyd. Deepfloyd if. <https://huggingface.co/DeepFloyd>, 2023.

Deng, C., Zhu, D., Li, K., Gou, C., Li, F., Wang, Z., Zhong, S., Yu, W., Nie, X., Song, Z., et al. Emerging properties in unified multimodal pretraining. *arXiv preprint arXiv:2505.14683*, 2025.

Desync. Perfect deliberate. <https://civitai.com/models/24350/perfectdeliberate>, 2024.

Devlin, J., Chang, M.-W., Lee, K., and Toutanova, K. Bert: Pre-training of deep bidirectional transformers for language understanding. In *Proceedings of the 2019 conference of the North American chapter of the association for computational linguistics: human language technologies, volume 1 (long and short papers)*, pp. 4171–4186, 2019.

Esser, P., Rombach, R., and Ommer, B. Taming transformers for high-resolution image synthesis. In *Proceedings of the IEEE/CVF conference on computer vision and pattern recognition*, pp. 12873–12883, 2021.

Esser, P., Kulal, S., Blattmann, A., Entezari, R., Müller, J., Saini, H., Levi, Y., Lorenz, D., Sauer, A., Boesel, F., et al. Scaling rectified flow transformers for high-resolution image synthesis. In *Forty-first international conference on machine learning*, 2024.

Fan, Y., Watkins, O., Du, Y., Liu, H., Ryu, M., Boutilier, C., Abbeel, P., Ghavamzadeh, M., Lee, K., and Lee, K. Dpok: Reinforcement learning for fine-tuning text-to-image diffusion models. *Advances in Neural Information Processing Systems*, 36:79858–79885, 2023.

Fang, R., Duan, C., Wang, K., Huang, L., Li, H., Yan, S., Tian, H., Zeng, X., Zhao, R., Dai, J., et al. Got: Unleashing reasoning capability of multimodal large language model for visual generation and editing. *arXiv preprint arXiv:2503.10639*, 2025.

Ghosh, D., Hajishirzi, H., and Schmidt, L. Geneval: An object-focused framework for evaluating text-to-image alignment. *Advances in Neural Information Processing Systems*, 36:52132–52152, 2023.

Ho, J., Jain, A., and Abbeel, P. Denoising diffusion probabilistic models. *Advances in neural information processing systems*, 33:6840–6851, 2020.

Hu, X., Wang, R., Fang, Y., Fu, B., Cheng, P., and Yu, G. Ella: Equip diffusion models with llm for enhanced semantic alignment. *arXiv preprint arXiv:2403.05135*, 2024.

Huang, Z., Chen, Z., Wang, Z., Li, T., and Qi, G.-J. Reinforcing the diffusion chain of lateral thought with diffusion language models. *arXiv preprint arXiv:2505.10446*, 2025.

Ilharco, G., Wortsman, M., Wightman, R., Gordon, C., Carlini, N., Taori, R., Dave, A., Shankar, V., Namkoong, H., Miller, J., Hajishirzi, H., Farhadi, A., and Schmidt, L. Openclip, July 2021. URL <https://doi.org/10.5281/zenodo.5143773>. If you use this software, please cite it as below.

Kim, D., He, J., Yu, Q., Yang, C., Shen, X., Kwak, S., and Chen, L.-C. Democratizing text-to-image masked generative models with compact text-aware one-dimensional tokens. *arXiv preprint arXiv:2501.07730*, 2025.

Lee, D., Kim, C., Kim, S., Cho, M., and Han, W.-S. Autoregressive image generation using residual quantization. In *Proceedings of the IEEE/CVF conference on computer vision and pattern recognition*, pp. 11523–11532, 2022.

Lee, H., Phatale, S., Mansoor, H., Mesnard, T., Ferret, J., Lu, K., Bishop, C., Hall, E., Carbune, V., Rastogi, A., et al. Rlaif vs. rlhf: Scaling reinforcement learning from human feedback with ai feedback. *arXiv preprint arXiv:2309.00267*, 2023.

Li, T., Chang, H., Mishra, S., Zhang, H., Katabi, D., and Krishnan, D. Mage: Masked generative encoder to unify representation learning and image synthesis. In *Proceedings of the IEEE/CVF Conference on Computer Vision and Pattern Recognition*, pp. 2142–2152, 2023.

Li, T., Tian, Y., Li, H., Deng, M., and He, K. Autoregressive image generation without vector quantization. *Advances in Neural Information Processing Systems*, 37:56424–56445, 2024.

Liang, Z., Yuan, Y., Gu, S., Chen, B., Hang, T., Li, J., and Zheng, L. Step-aware preference optimization: Aligning preference with denoising performance at each step. *arXiv preprint arXiv:2406.04314*, 2(5):7, 2024.

Liang, Z., Li, Y., Yang, T., Wu, C., Mao, S., Pei, L., Yang, X., Pang, J., Mu, Y., and Luo, P. Discrete diffusion vla: Bringing discrete diffusion to action decoding in vision-language-action policies. *arXiv preprint arXiv:2508.20072*, 2025.

Lipman, Y., Chen, R. T., Ben-Hamu, H., Nickel, M., and Le, M. Flow matching for generative modeling. *arXiv preprint arXiv:2210.02747*, 2022.

Liu, B., Akhgari, E., Visheratin, A., Kamko, A., Xu, L., Shrira, S., Lambert, C., Souza, J., Doshi, S., and Li, D. Playgroud v3: Improving text-to-image alignment with deep-fusion large language models. *arXiv preprint arXiv:2409.10695*, 2024.

Liu, J., Liu, G., Liang, J., Li, Y., Liu, J., Wang, X., Wan, P., Zhang, D., and Ouyang, W. Flow-grpo: Training flow matching models via online rl. *arXiv preprint arXiv:2505.05470*, 2025.

Liu, X., Gong, C., and Liu, Q. Flow straight and fast: Learning to generate and transfer data with rectified flow. *arXiv preprint arXiv:2209.03003*, 2022.

Luo, S., Tan, Y., Huang, L., Li, J., and Zhao, H. Latent consistency models: Synthesizing high-resolution images with few-step inference. *arXiv preprint arXiv:2310.04378*, 2023.

Luo, Y., Hu, X., Fan, K., Sun, H., Chen, Z., Xia, B., Zhang, T., Chang, Y., and Wang, X. Reinforcement learning meets masked generative models: Mask-grpo for text-to-image generation. *arXiv preprint arXiv:2510.13418*, 2025.

Merjic. Majicmix realistic v7. <https://civitai.com/models/43331?modelVersionId=176425>, 2023.

Ni, Z., Wang, Y., Zhou, R., Guo, J., Hu, J., Liu, Z., Song, S., Yao, Y., and Huang, G. Revisiting non-autoregressive transformers for efficient image synthesis. In *Proceedings of the IEEE/CVF Conference on Computer Vision and Pattern Recognition*, pp. 7007–7016, 2024a.

Ni, Z., Wang, Y., Zhou, R., Han, Y., Guo, J., Liu, Z., Yao, Y., and Huang, G. Enat: rethinking spatial-temporal interactions in token-based image synthesis. In *Proceedings of the 38th International Conference on Neural Information Processing Systems*, NIPS ’24, Red Hook, NY, USA, 2024b. Curran Associates Inc. ISBN 9798331314385.

Ni, Z., Wang, Y., Zhou, R., Lu, R., Guo, J., Hu, J., Liu, Z., Yao, Y., and Huang, G. Adanat: Exploring adaptive policy for token-based image generation. In *European Conference on Computer Vision*, pp. 302–319. Springer, 2024c.

Ni, Z., Wang, Y., Hua, Y., Zhou, R., Guo, J., Song, J., Zheng, B., and Huang, G. Adagen: Learning adaptive policy for image synthesis. *IEEE Transactions on Pattern Analysis and Machine Intelligence*, pp. 1–18, 2025. doi: 10.1109/TPAMI.2025.3626772.

Nie, S., Zhu, F., You, Z., Zhang, X., Ou, J., Hu, J., Zhou, J., Lin, Y., Wen, J.-R., and Li, C. Large language diffusion models. *arXiv preprint arXiv:2502.09992*, 2025.

Parmar, N., Vaswani, A., Uszkoreit, J., Kaiser, L., Shazeer, N., Ku, A., and Tran, D. Image transformer. In *International conference on machine learning*, pp. 4055–4064. PMLR, 2018.

Peebles, W. and Xie, S. Scalable diffusion models with transformers. In *Proceedings of the IEEE/CVF international conference on computer vision*, pp. 4195–4205, 2023a.

Peebles, W. and Xie, S. Scalable diffusion models with transformers. In *Proceedings of the IEEE/CVF international conference on computer vision*, pp. 4195–4205, 2023b.

Perez, E., Strub, F., De Vries, H., Dumoulin, V., and Courville, A. Film: Visual reasoning with a general conditioning layer. In *Proceedings of the AAAI conference on artificial intelligence*, volume 32, 2018.

Podell, D., English, Z., Lacey, K., Blattmann, A., Dockhorn, T., Müller, J., Penna, J., and Rombach, R. Sdxl: Improving latent diffusion models for high-resolution image synthesis. *arXiv preprint arXiv:2307.01952*, 2023.

Radford, A., Kim, J. W., Hallacy, C., Ramesh, A., Goh, G., Agarwal, S., Sastry, G., Askell, A., Mishkin, P., Clark, J., Krueger, G., and Sutskever, I. Learning transferable visual models from natural language supervision. In *ICML*, 2021.

Rafailov, R., Sharma, A., Mitchell, E., Manning, C. D., Ermon, S., and Finn, C. Direct preference optimization: Your language model is secretly a reward model. *Advances in neural information processing systems*, 36: 53728–53741, 2023.

Ramesh, A., Dhariwal, P., Nichol, A., Chu, C., and Chen, M. Hierarchical text-conditional image generation with clip latents. *arXiv preprint arXiv:2204.06125*, 1(2):3, 2022.

Razavi, A., Van den Oord, A., and Vinyals, O. Generating diverse high-fidelity images with vq-vae-2. *Advances in neural information processing systems*, 32, 2019.

Rombach, R., Blattmann, A., Lorenz, D., Esser, P., and Ommer, B. High-resolution image synthesis with latent diffusion models. In *Proceedings of the IEEE/CVF conference on computer vision and pattern recognition*, pp. 10684–10695, 2022.

Saharia, C., Chan, W., Saxena, S., Li, L., Whang, J., Denton, E. L., Ghasemipour, K., Gontijo Lopes, R., Karagol Ayan, B., Salimans, T., et al. Photorealistic text-to-image diffusion models with deep language understanding. *Advances in neural information processing systems*, 35:36479–36494, 2022.

Schulman, J., Wolski, F., Dhariwal, P., Radford, A., and Klimov, O. Proximal policy optimization algorithms. *arXiv preprint arXiv:1707.06347*, 2017.

SG_161222. Realvisxl v5.0. <https://civitai.com/models/139562/realvisxl-v50>, 2024.

Shao, Z., Wang, P., Zhu, Q., Xu, R., Song, J., Bi, X., Zhang, H., Zhang, M., Li, Y., Wu, Y., et al. Deepseekmath: Pushing the limits of mathematical reasoning in open language models. *arXiv preprint arXiv:2402.03300*, 2024.

Sun, H., Wu, J., Xia, B., Luo, Y., Zhao, Y., Qin, K., Lv, X., Zhang, T., Chang, Y., and Wang, X. Reinforcement fine-tuning powers reasoning capability of multimodal large language models. *arXiv preprint arXiv:2505.18536*, 2025.

Sun, P., Jiang, Y., Chen, S., Zhang, S., Peng, B., Luo, P., and Yuan, Z. Autoregressive model beats diffusion: Llama for scalable image generation. *arXiv preprint arXiv:2406.06525*, 2024.

Team, C. Chameleon: Mixed-modal early-fusion foundation models. *arXiv e-prints*, pp. arXiv–2405, 2024.

Wallace, B., Dang, M., Rafailov, R., Zhou, L., Lou, A., Purushwalkam, S., Ermon, S., Xiong, C., Joty, S., and Naik, N. Diffusion model alignment using direct preference optimization. In *Proceedings of the IEEE/CVF Conference on Computer Vision and Pattern Recognition*, pp. 8228–8238, 2024.

Wang, J., Tian, Z., Wang, X., Zhang, X., Huang, W., Wu, Z., and Jiang, Y.-G. Simplear: Pushing the frontier of autoregressive visual generation through pretraining, sft, and rl. *arXiv preprint arXiv:2504.11455*, 2025a.

Wang, Y., Yue, Y., Yue, Y., Wang, H., Jiang, H., Han, Y., Ni, Z., Pu, Y., Shi, M., Lu, R., et al. Emulating human-like adaptive vision for efficient and flexible machine visual perception. *Nature Machine Intelligence*, pp. 1–19, 2025b.

Wu, C., Chen, X., Wu, Z., Ma, Y., Liu, X., Pan, Z., Liu, W., Xie, Z., Yu, X., Ruan, C., et al. Janus: Decoupling visual encoding for unified multimodal understanding and generation. In *Proceedings of the Computer Vision and Pattern Recognition Conference*, pp. 12966–12977, 2025.

Wu, X., Hao, Y., Sun, K., Chen, Y., Zhu, F., Zhao, R., and Li, H. Human preference score v2: A solid benchmark for evaluating human preferences of text-to-image synthesis. *arXiv preprint arXiv:2306.09341*, 2023.

Xiao, S., Wang, Y., Zhou, J., Yuan, H., Xing, X., Yan, R., Li, C., Wang, S., Huang, T., and Liu, Z. Omnigen: Unified image generation. In *Proceedings of the Computer Vision and Pattern Recognition Conference*, pp. 13294–13304, 2025.

Xie, J., Mao, W., Bai, Z., Zhang, D. J., Wang, W., Lin, K. Q., Gu, Y., Chen, Z., Yang, Z., and Shou, M. Z. Show-o: One single transformer to unify multimodal understanding and generation. *arXiv preprint arXiv:2408.12528*, 2024a.

Xie, J., Mao, W., Bai, Z., Zhang, D. J., Wang, W., Lin, K. Q., Gu, Y., Chen, Z., Yang, Z., and Shou, M. Z. Show-o: One single transformer to unify multimodal understanding and generation. *arXiv preprint arXiv:2408.12528*, 2024b.

Xu, J., Liu, X., Wu, Y., Tong, Y., Li, Q., Ding, M., Tang, J., and Dong, Y. Imagereward: Learning and evaluating human preferences for text-to-image generation. *Advances in Neural Information Processing Systems*, 36: 15903–15935, 2023.

Xue, Z., Wu, J., Gao, Y., Kong, F., Zhu, L., Chen, M., Liu, Z., Liu, W., Guo, Q., Huang, W., et al. Dancegrpo: Unleashing grpo on visual generation. *arXiv preprint arXiv:2505.07818*, 2025.

Yang, L., Tian, Y., Li, B., Zhang, X., Shen, K., Tong, Y., and Wang, M. Mmada: Multimodal large diffusion language models. *arXiv preprint arXiv:2505.15809*, 2025.

Ye, J., Xie, Z., Zheng, L., Gao, J., Wu, Z., Jiang, X., Li, Z., and Kong, L. Dream 7b: Diffusion large language models. *arXiv preprint arXiv:2508.15487*, 2025.

You, Z., Nie, S., Zhang, X., Hu, J., Zhou, J., Lu, Z., Wen, J.-R., and Li, C. Llada-v: Large language diffusion models with visual instruction tuning. *arXiv preprint arXiv:2505.16933*, 2025.

Yuan, H., Chen, Z., Ji, K., and Gu, Q. Self-play fine-tuning of diffusion models for text-to-image generation. *Advances in Neural Information Processing Systems*, 37:73366–73398, 2024.

Zhang, S., Wang, B., Wu, J., Li, Y., Gao, T., Zhang, D., and Wang, Z. Learning multi-dimensional human preference for text-to-image generation. In *Proceedings of the IEEE/CVF Conference on Computer Vision and Pattern Recognition*, pp. 8018–8027, 2024.

Zhang, T., Da, C., Ding, K., Yang, H., Jin, K., Li, Y., Gao, T., Zhang, D., Xiang, S., and Pan, C. Diffusion model as a noise-aware latent reward model for step-level preference optimization. *arXiv preprint arXiv:2502.01051*, 2025.

Zhu, F., Wang, R., Nie, S., Zhang, X., Wu, C., Hu, J., Zhou, J., Chen, J., Lin, Y., Wen, J.-R., et al. Llada 1.5: Variance-reduced preference optimization for large language diffusion models. *arXiv preprint arXiv:2505.19223*, 2025.

Appendix

A. More Implementation Details

Dataset. We conduct our experiments using a mixture of prompts from the HPDv2 (Wu et al., 2023) and ImageReward (Xu et al., 2023) datasets’ training splits, consisting of 103,700 and 8,000 prompts respectively. We use only the text prompts from these datasets without their corresponding images.

Model architecture. Following Meissonic (Bai et al., 2024), our text encoder is CLIP-ViT-H-14 from Open-CLIP (Radford et al., 2021), which remains frozen during training. Our scheduling policy network consists of a depthwise convolution layer, a pointwise convolution layer, and a multi-layer perceptron (MLP). We extract visual token features from the final layer output of the transformer blocks and incorporate timestep information into the policy network using adaptive layer normalization (AdaLN) (Peebles & Xie, 2023b; Perez et al., 2018).

Training settings. We optimized both policies with Adam ($\beta_1 = 0.9, \beta_2 = 0.95$). The 1.0B-parameter model policy was trained for 300 iterations with learning rate 1×10^{-5} , weight-decay 0.02, group size $G = 6$, and total batch size 96. The 9M-parameter Scheduling Policy was trained for 200 iterations with learning rate 1×10^{-4} , weight decay 0, $G = 8$, and total batch size 256. Its lighter architecture enabled faster convergence.

B. Comparison Across Inference Steps

We conduct a comparative analysis between the Meissonic base model and our Co-GRPO method by varying the number of inference steps from 8 to 64. All results are evaluated using the same checkpoint trained with 48 steps; only the inference step count is varied at test time. We measure the overall inference time with batch size 4 on an NVIDIA A100 (40GB). Notably, the reported inference times for Co-GRPO include the computational overhead of the scheduling policy network. The number of parameters of the scheduling policy is less than 1% of the base model’s, resulting in negligible forward pass latency that does not substantially affect overall inference time.

As illustrated in Figure 5, Co-GRPO consistently improves ImageReward scores across all step counts, demonstrating that the learned scheduling policy effectively reallocates computational resources to the most informative timesteps. Specifically, while the baseline model requires 48 steps to achieve an ImageReward of 0.94, Co-GRPO attains the same performance with fewer than 16 steps, representing a great reduction of over required inference steps.

C. Visualization Results

C.1. Prompts used for Teaser Figure

We present the prompts used for the teaser figure in Table 6.

C.2. More Visualization Results

Additional images generated by our Co-GRPO method are shown in Figure 6. All of the prompts are selected from ImageReward and HPDv2 test splits.

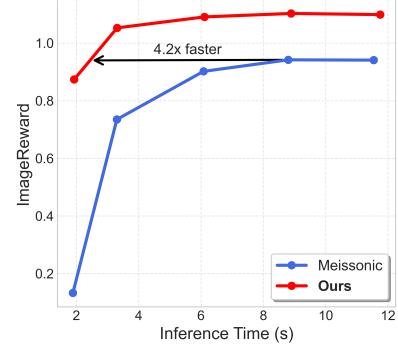


Figure 5: **Comparison between Meissonic base model and our Co-GRPO trained model across different steps.** Our Co-GRPO improves the performance of the model over every steps, with a 4.2 times faster compared to the base model on the same score.

Column	Prompts
1	The woman sitting at the table looks bored.
2	A digital painting of a beautiful creature in intricate detail, centered in a low angle shot.
3	US Air Force battling against the Rebellion in a radioactive environment with detailed digital artwork.
4	The sea, sunset, colorful, clear water, digital illustration.
5	The image is a cinematic portrait of Walt Whitman depicted as a bodhisattva in the style of several famous artists, painted in oil on canvas or gouache with intricate details and desaturated colors.

Table 6: Prompts employed in the teaser examples generation.

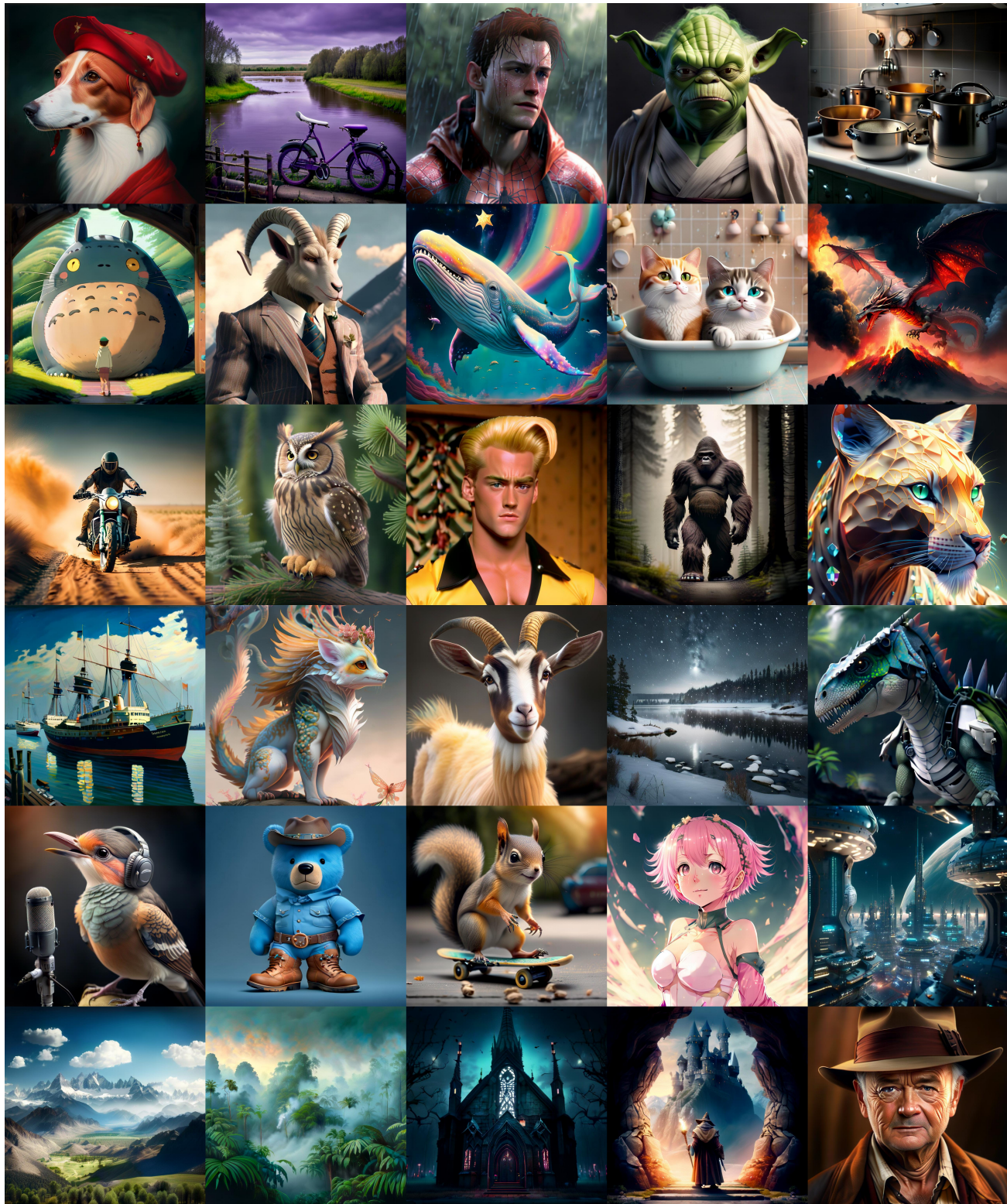


Figure 6: Representative high-quality images generated by our Co-GRPO method.